How to cite: *Angew. Chem. Int. Ed.* **2024**, *63*, e202410646
doi.org/10.1002/anie.202410646

Ethylene Dimerization

Highly Efficient Low-loaded $PdO_x/AlSiO_x$ Catalyst for Ethylene Dimerization

Tatiana Otroshchenko, Dmitry I. Sharapa,* Elizaveta A. Fedorova, Dan Zhao, and Evgenii V. Kondratenko*

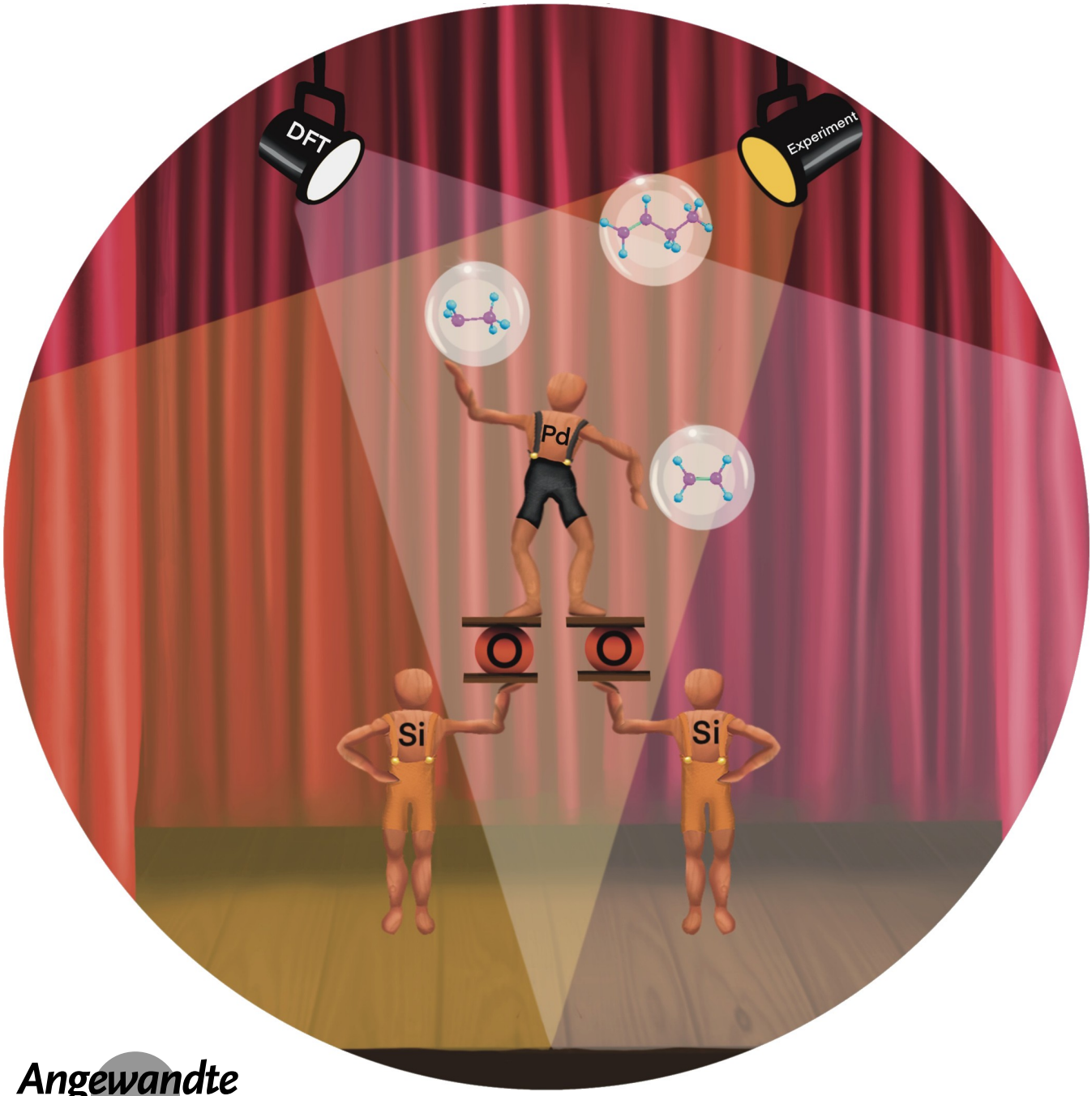

Abstract: Ethylene dimerization is an industrial process that is currently carried out using homogeneous catalysts. Here we present a highly active heterogeneous catalyst containing minute amounts of atomically dispersed Pd. It requires no co-catalyst(s) or activator(s) and significantly outperforms previously reported catalysts tested under similar reaction conditions. The selectivity to C_4- and C_6-hydrocarbons was about 80 % and 10 % at 42 % ethylene conversion at 200 °C using an industrially relevant feed containing 50 vol % ethylene, respectively. Our kinetic and catalyst characterization experiments complemented by density functional theory calculations provide molecular insights into the local environment of isolated $Pd(II)O_x$ species and their role in achieving high activity in the target reaction. When the developed catalyst was rationally integrated with a Mo-containing olefin metathesis catalyst in the same reactor, the formed butenes reacted with ethylene to propylene with a selectivity of 98 % at about 24 % ethylene conversion.

Introduction

Ethylene dimerization is an important industrial process to produce higher molecular weight olefins applied for the manufacture of polymers and other valuable chemicals (detergents, plasticizers, lubricants, surfactants, jet fuels, etc.).[1] This process is also attractive from a sustainable point of view because ethylene can be produced from bioethanol.[2] Commercial dimerization processes are carried out in a liquid phase in the presence of homogeneous catalysts on the basis of transition metal (Ni, Ti, Zr, Cr, Co, Fe) complexes and alkylaluminium co-catalysts.[3] Although the catalysts developed show high activity, their separation from the products, recycling and regeneration are rather complicated and inefficient or expensive. Therefore, considering the main principles of green chemistry, the development of environmentally friendly heterogeneous dimerization catalysts has attracted great attention in both academia and industry.[4]

The most promising heterogeneous catalysts reported so far include (i) metal complexes immobilized on polymers and oxides,[5] (ii) metal–organic framework materials,[6] and (iii) transition metals supported on inorganic porous materials.[3,7] While the catalysts from groups (i) and (ii) have doubtful perspectives for a large-scale application due to their complex preparation and regeneration procedures as well as the requirement of the presence of co-catalyst in most cases, the group (iii) catalysts have a promising potential. In this regard, catalysts with NiO_x species dispersed on different support materials (silica, alumina, amorphous aluminosilicates, zeolites, zirconia etc.) have been widely investigated.[7–8] Although Rh-, Ru-, or Pd-exchanged zeolites are also known to be active for ethylene dimerization,[9] they have not attracted much interest in the scientific community. Accordingly, the prospects and mechanistic insights of ethylene dimerization over catalysts based on Pt-group metals (PGMs) remain unexplored.

Herein, we demonstrate highly efficient ethylene dimerization over a heterogeneous catalyst containing only tiny amounts of Pd (0.1 wt %) to meet the requirements for large-scale applications due to the scarcity and high price of the metal. By combining state-of-the-art characterization methods with kinetic and theoretical analyses, isolated $Pd(II)O_x$ species were found to exhibit unexpectedly high dimerization performance. The fundamentals of their formation were also elucidated. Finally, we show that nearly 100 % selective propylene production was achieved when feeding ethylene to a reactor filled with the developed dimerization catalyst and a Mo-containing olefin metathesis catalyst with the latter being as a downstream layer.

Results and Discussion

Since the presence of Brønsted acidic sites is often reported to be critical for achieving high metal dispersion,[10] a commercial aluminosilicate (Siral 40, 40 wt % SiO_2 in Al_2O_3, from SASOL) possessing high amount of Brønsted acidic sites of middle strength was applied as support material for the catalyst preparation. Noticeably, this support but not zeolites was used since the microporous character and strong acidity of the latter materials can cause rapid catalyst deactivation. Calcined Siral 40 support (XRD pattern is shown in Figure S1) was impregnated with an aqueous solution of Ru, Rh, Ir, Pt, or Pd precursor according to an incipient wetness impregnation method (see "Catalyst preparation" in the Supporting Information). The nominal surface density of each metal was set to 0.013 atoms per 1 nm^2. In addition, a reference Ni-based catalyst with the same Ni surface density was synthesized. The actual metal content determined after calcination of the catalyst precursors at 500 °C does not differ significantly from the nominal value (Table S1).

To understand how the supported species were formed, the bare support and the catalysts were characterized by diffuse reflectance infrared Fourier transformation spectro-

[*] Dr. T. Otroshchenko, Dr. E. A. Fedorova, Prof. Dr. E. V. Kondratenko
Department of Advanced Methods for Applied Catalysis
Leibniz-Institut für Katalyse e.V. (LIKAT)
Albert-Einstein-Str. 29a, D-18059 Rostock, Germany
E-mail: tatiana.otroshchenko@catalysis.de
Dr. D. I. Sharapa, Dr. D. Zhao
Institute of Catalysis Research and Technology, Karlsruhe Institute of Technology (KIT),
Hermann-von-Helmholtz-Platz 1, 76344, Eggenstein-Leopoldshafen, Germany
E-mail: dmitry.sharapa@kit.edu

scopy (DRIFTS) and temperature-programmed desorption of adsorbed NH_3 (NH_3-TPD). All dehydrated support samples contain isolated Si–OH groups and hydrogen-bonded vicinal hydroxyls characterized by sharp and broad bands at 3741 and 3600 cm^{-1} in the DRIFT spectra, respectively[11] (Figure S2). However, the I_{3600}/I_{3741} ratio (where I_{3600} is the intensity of the band at 3600 cm^{-1} and I_{3741} is the intensity of the band at 3741 cm^{-1}) decreased after deposition of the metal species. This result suggests that the vicinal support hydroxyls were preferentially consumed for anchoring metal precursors. The hydroxyls should be Brønsted acidic sites, since the total acidity of the catalysts is lower compared to the support as demonstrated by NH_3-TPD (Table S1, Figure S3).

All samples were tested in ethylene dimerization at 200 °C and 1.25 bar in a continuous-flow fixed-bed reactor (see the Supporting Information for details). The ethylene conversion and product selectivity obtained after 14 min on reaction stream are shown in Figure 1. The Pd/Siral 40 catalyst achieved the selectivity to butenes of about 80 % at 42 % ethylene conversion. The conversion over other samples did not exceed 2 %. Moreover, the best-performing catalyst showed several orders of magnitude higher metal-related activity in comparison with state-of-the-art heterogeneous catalysts tested in fixed-bed reactors without co-catalyst (Table S2).

The operando UV/Vis spectrum of Pd/Siral 40 at 200 °C changes significantly with increasing time on ethylene stream (Figure 2 (a), (b)). The appearance of the bands at 305, 380 and 425 nm can be related to the formation of adsorbed carbon-containing species (coke precursors) on the catalyst surface. It is noteworthy that no decrease in the ethylene conversion was observed during the whole experiment (Figure 2 (c), (d)), implying that acidic support but not the active Pd-containing sites is preferentially covered by coke precursors. Indeed, the intensities of the same bands slowly increased when bare Siral 40 was treated with ethylene (Figure S4 (a)–(c)). The temporal changes in the UV/Vis spectrum of bare Siral 40 were more pronounced when ethylene was replaced by 2-butene (the main product formed from ethylene over Pd/Siral 40) and looked similar to those observed for Pd/Siral 40 (Figure S4 (d), (e) versus Figure 2 (a), (b)). Thus, due to their stronger adsorption on the catalyst surface, oligomerization products but not ethylene should be the main precursors of coke deposits. Such assumption is further supported by the in situ DRIFTS experiments (Figure S5 and the related discussion below this Figure).

To derive further insights into primary and secondary reaction pathways in the course of ethylene dimerization over Pd/Siral 40 at 200 °C, we performed catalytic tests at different contact times but constant temperature to achieve different degrees of ethylene conversion. The contact time was varied by both changing catalyst amount and total flow. The obtained dependences of selectivity to butenes, hexenes, octenes and coke on ethylene conversion are shown in Figure 3 (a). The selectivity to butenes decreases from 97 to 80 % with increasing ethylene conversion from 9 to 42 % thus implying the presence of a sequential stage(s) involving these products. Extrapolation to zero conversion degree gives near to 100 % selectivity to butenes. This means that they are the only products formed directly from ethylene under the applied reaction conditions. The selectivity to other products (hexenes, octenes, coke) starts from zero at zero ethylene conversion and increases with increasing conversion. Such behavior implies that these products are formed via sequential stages involving butenes. Accordingly, based on the above discussion, we suggest a reaction network of ethylene transformation over Pd/Siral 40 at 200 °C that is shown in Figure 3 (b).

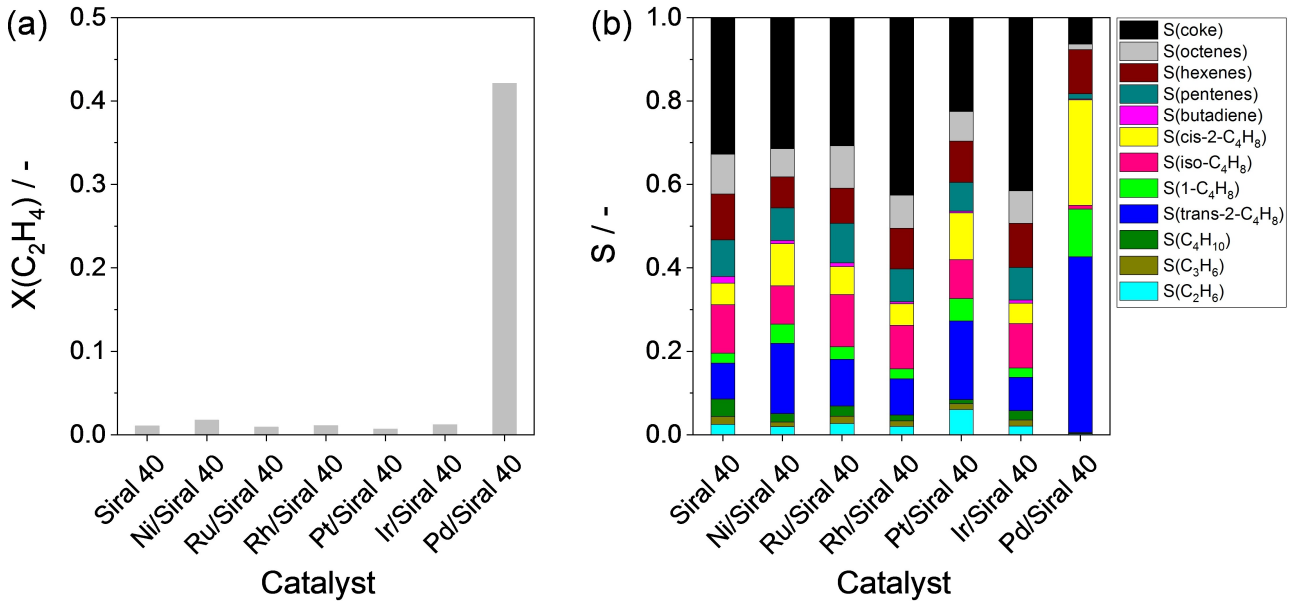

Figure 1. (a) Ethylene conversion ($X(C_2H_4)$) and (b) product selectivity (S) over different catalysts. Reaction conditions: 50 vol.% C_2H_4 in N_2, total flow = 20 mL·min^{-1}, total pressure = 1.25 bar, m = 200 mg, T = 200 °C.

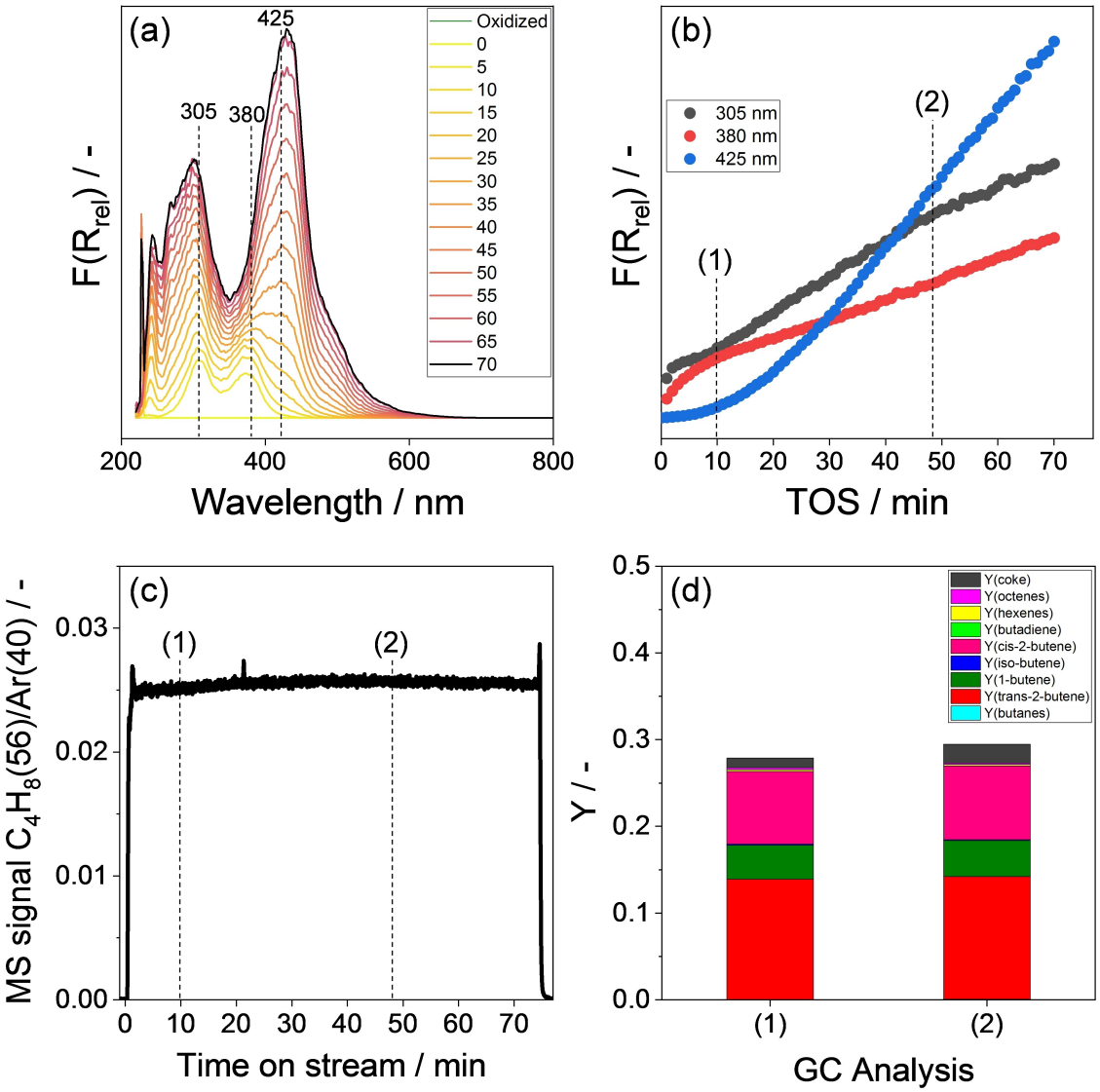

Figure 2. (a) UV/Vis spectra ($F(R_{rel})$) of Pd/Siral 40 after different times on ethylene stream (50 vol.% C_2H_4 in Ar) at 200 °C; (b) temporal changes in $F(R_{rel})$ at 305, 380 and 425 nm during treatment in ethylene; (c) normalized MS signal of C_4H_8 (m/z = 56) collected during exposing of Pd/Siral 40 to ethylene at 200 °C; (d) product yields calculated for Pd/Siral 40 from the data of two GC analyses made after 10 and 48 min on ethylene stream at 200 °C.

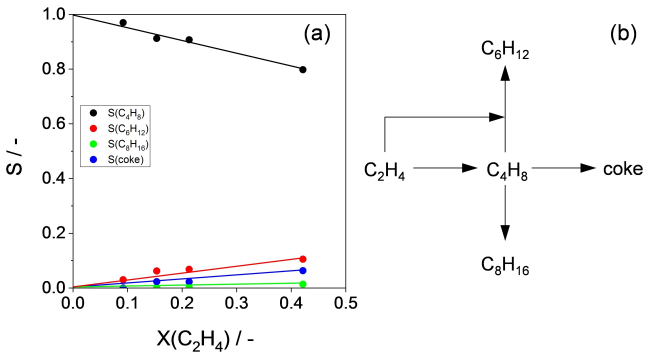

Figure 3. (a) Dependence of selectivity to butenes, hexenes, octenes and coke on ethylene conversion determined over Pd/Siral 40 at 200 °C and (b) proposed Scheme of product formation in the course of ethylene dimerization.

Although 1-C_4H_8 should be formed exclusively according to the most accepted metallocene or Cossee-Arlman mechanisms of ethylene dimerization,[12] all butene isomers (1-C_4H_8, *trans*- and *cis*-2-C_4H_8, iso-C_4H_8) were observed during ethylene dimerization over Pd/Siral 40, with the fraction of *trans*-2-C_4H_8 being the highest one (Figure 1 (b), Figure 2 (d)). This can be explained by the strong ability of Siral 40 to isomerize primarily formed 1-C_4H_8. In a control experiment, all butene isomers were formed, when 1-C_4H_8 reacted with bare Siral 40 or Pd/Siral 40 at 200 °C (Figure S6).

To identify the origin of the unexpectedly high activity of the Pd/Siral 40 catalyst, this material was characterized by X-ray photoelectron spectroscopy (XPS), aberration-corrected high angle annular dark-field scanning transmission electron microscopy (AC-HAADF-STEM), X-ray absorp-

tion spectroscopy (XAS), and diffuse reflectance UV/Vis spectroscopy.

No XP signal related to Pd could be identified due to the very low metal content (Figure S7). Based on the AC-HAADF-STEM images (Figure 4 (a)–(d)), the presence of Pd or PdO_x nanoparticles can be excluded. The catalyst surface is populated by highly dispersed sub-nanosized clusters and isolated Pd single atoms.

From the ex situ X-ray absorption near-edge structure (XANES) spectra (Figure 4 (e)), the absorption edge peak of Pd/Siral 40 is shifted towards higher energies compared to that of Pd foil. The spectrum of Pd/Siral 40 is very similar to that of the $PdSO_4 \cdot H_2O$ reference, indicating the presence of Pd(II) species in the catalyst. The Fourier-transformed (FT) k^2-weighted extended X-ray absorption fine structure (EXAFS) spectrum of Pd/Siral 40 has the only distinct peak at 1.5 Å, which is typical for the first coordination shell of Pd in a bonding configuration of Pd–O as can be seen in the corresponding spectra of the PdO and $PdSO_4 \cdot H_2O$ references (Figure 4 (f)). The absence of the peaks corresponding to the first shell Pd–Pd coordination typical for Pd foil (peak at 2.6 Å) and to the second shell Pd–Pd coordination characteristic for PdO (peak at 2.9 Å) indicates that the most part of Pd in Pd/Siral 40 is present in the form of isolated PdO_x single sites. The Fourier-transformed EXAFS spectrum of Pd/Siral 40 was fitted with a model using first-shell coordination to oxygen (Figure S8). The obtained Pd–O coordination number was 3.5 (Table S3). It should be however mentioned that the spectra were collected ex situ using a high catalyst amount (100 mg). An attempt to collect in situ XAS data for freshly calcined catalysts failed due to the limited reactor volume which is not enough to use high amount of the catalyst with low Pd loading. Thus, the experiments performed ex situ cannot exclude that atmospheric water did not interact with PdO_x species. Such interaction may influence the Pd–O coordination number. The presence of adsorbed water species was experimentally proven by in situ diffuse reflectance Fourier-transform infrared spectroscopy. These species can be removed through high-temperature treatment in air (Figure S9 (a)). We also found that the non-treated catalyst demonstrates more than 9 times lower activity compared to its in situ calcined counterpart (Figure S9 (b)). Accordingly, we suppose that the calcination step can lead to a change in the local structure of the PdO_x species and a decrease in the Pd–O coordination number due to the removal of water.

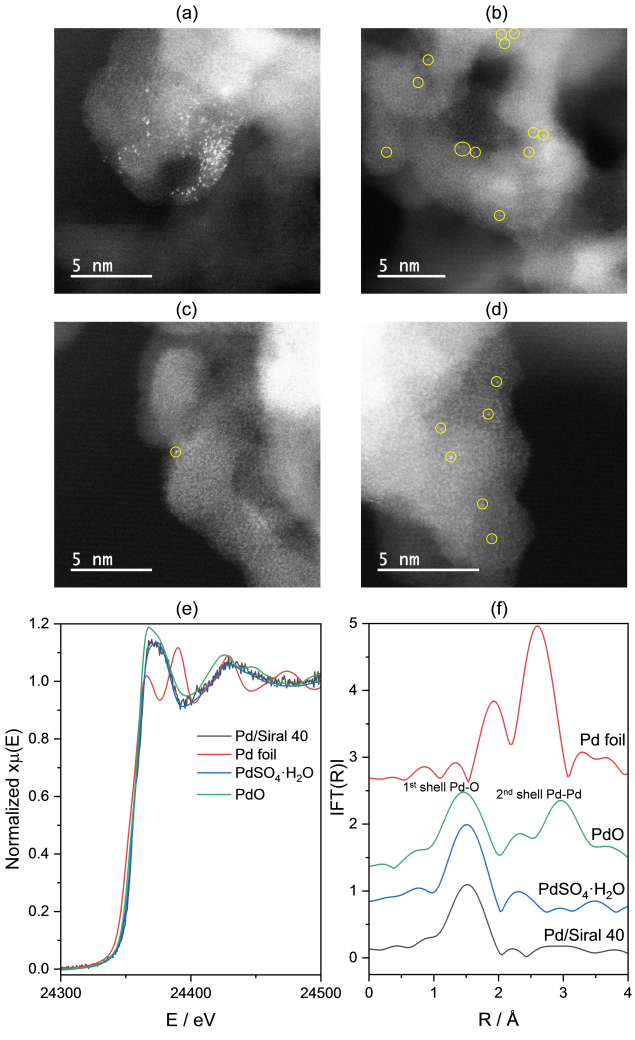

Figure 4. Structural characterizations of Pd/Siral 40: (a)–(d) Sequence of AC-HAADF-STEM images obtained for Pd/Siral 40 showing highly dispersed/isolated Pd (in yellow circles); Pd K-edge (e) XANES and (f) EXAFS spectra of Pd/Siral 40 sample, Pd foil, PdO and $PdSO_4 \cdot H_2O$.

The UV/Vis spectrum of Pd/Siral 40 in air at 200 °C is characterized by intense absorption bands at 247 nm and at 450 nm (Figure S10 (a)). They can be assigned to oxygen charge transfer (O^{2-} to Pd^{2+}) and d–d transitions of Pd^{2+} respectively in highly dispersed $Pd(II)O_x$ species bound to the support via oxygen.[13] Such species are readily converted to metallic Pd^0 during catalyst treatment in an H_2-containing flow at 200 °C as concluded from the appearance of absorption without a defined structure in a broad range of the spectrum (Figure S11 (a)).[13a] Importantly, the Pd/Siral 40 catalyst showed very low activity when treated in H_2 prior to ethylene dimerization (Figure S11 (b)). Therefore, highly dispersed $Pd(II)O_x$ species but not Pd^0 should be responsible for the target reaction. To confirm this assumption and to deepen our understanding of the nature of the active sites, we prepared reference Pd/SiO_2 and Pd/Al_2O_3 materials with the same Pd loading as in the Pd/Siral 40 catalyst (Table S1). They showed very low activity in ethylene dimerization (Figure S12). Inactivity of the Pd/SiO_2 catalyst can be explained by the presence of metallic Pd^0 in the fresh material (Figure S10 (b)). Although the UV/Vis spectra of Pd/Al_2O_3 and Pd/Siral 40 are similar due to the presence of highly dispersed $Pd(II)O_x$ species (Figure S10 (c)), the former catalyst is inactive. This discrepancy is due to the different local structure of these species as suggested by our DFT below.

DFT calculations were performed with the PBE functional using the VASP code to analyze ethylene dimerization according to both the Cossee-Arlman mechanism with the formation of ethyl species and the metallocene mechanism.[12,14] We focused on the C–C coupling step, which is considered to be rate-limiting.[15] The detailed

description of the proposed model for simulation of Siral 40 and basics of rational design of this model as well as details of DFT simulations and coordinates of all discussed species can be found in the Supporting Information (sections "Computational details" and "Coordinates of optimized structures").

Importantly, the chelation of Pd by the hydroxyls of the Siral 40 support provides a significant flexibility to the Pd(II) species, which can "stand up" or "lie down" making additional coordination with surface oxygen species (Figure S13). On the contrary, Pd(II) species in Pd/Al_2O_3 are arranged very much "in plane" (Figure S14). For both models, Pd(II) has a square coordination geometry when it contains two ligands (two ethylene molecules in the metallocene mechanism (Figure S15) or ethylene and ethyl group in the Cossee-Arlman mechanism (Figure 5). In the case of Pd/Al_2O_3, Pd(II) bends up, remaining bonded to only two oxygens and losing contact with two others.

In the Cossee-Arlman mechanism, the ethylene and ethyl group ligands couple to a butyl ligand, while Pd(II) bends to the surface and forms an additional bond with one (Pd/Siral 40) or two (Pd/Al_2O_3) surface oxygens (Figure 5). The transition state for Pd/Siral 40 (Figure 5, middle bottom structure) gives an activation energy of 0.59 eV (56.9 $kJ \cdot mol^{-1}$) or Gibbs free energy of 0.94 eV at 200 °C. The calculated activation energy is close to the apparent activation energy of 43.6 $kJ \cdot mol^{-1}$ determined experimentally in the temperature range between 100–200 °C (Figure S16). For Pd/Al_2O_3, the calculated barrier is 0.93 eV (the Gibbs free energy barrier is 1.21 eV). Accordingly, the difference in the ethylene dimerization activity between Pd/Siral 40 and Pd/Al_2O_3 observed in catalytic experiments could be due to the different local structure of the Pd(II) species.

The possibility of the C–C coupling via the metallocene mechanism was also considered (Figure S15). The obtained reaction barriers exceed 2 eV and thus this mechanism is unfavorable and can be excluded.

To demonstrate the feasibility of Pd/Siral 40 for the synthesis of propylene using an ethylene-containing feed, we have combined this catalyst with highly efficient Mo-based olefin metathesis catalyst (Mo/Siral 40) described elsewhere.[16] The top layer was the Pd/Siral 40 catalyst to generate butenes followed by their metathesis with ethylene over the downstream located Mo/Siral 40 catalyst. The reaction temperature was set to 150 °C. Pd/Siral 40 alone showed stable performance for at least 3 h on stream with ethylene conversion of about 15 % and selectivity to butenes of 96 % (Figure 6 (a)). The temporal changes of ethylene conversion and selectivity to butenes and propylene over the combination Pd/Siral 40 with Mo/Siral 40 are shown in Figure 6 (b). The initial ethylene conversion was 23.5 % and slightly increased to 24 %, selectivity to propylene increased

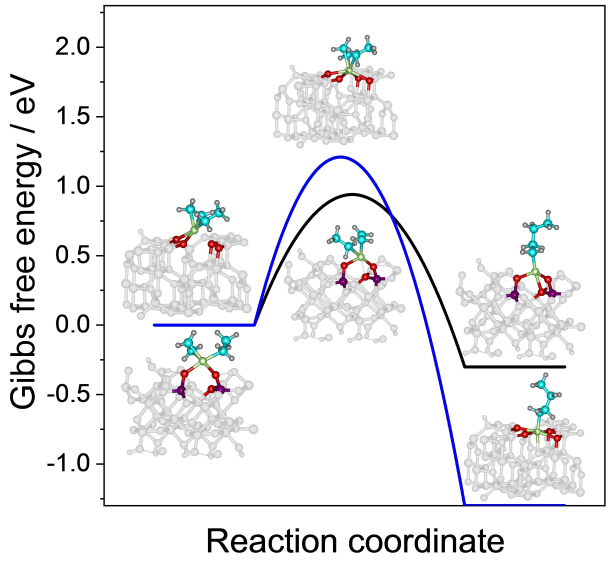

Figure 5. Gibbs free energy pathways calculated for C–C coupling in Cossee-Arlman ethylene dimerization over Pd/Siral 40 (black line) and Pd/Al_2O_3 (blue line) and the corresponding optimized structures of intermediates and transition states. Color scheme: Si – magenta, Pd – yellow, O – red, C – aqua, H – small silver grey.

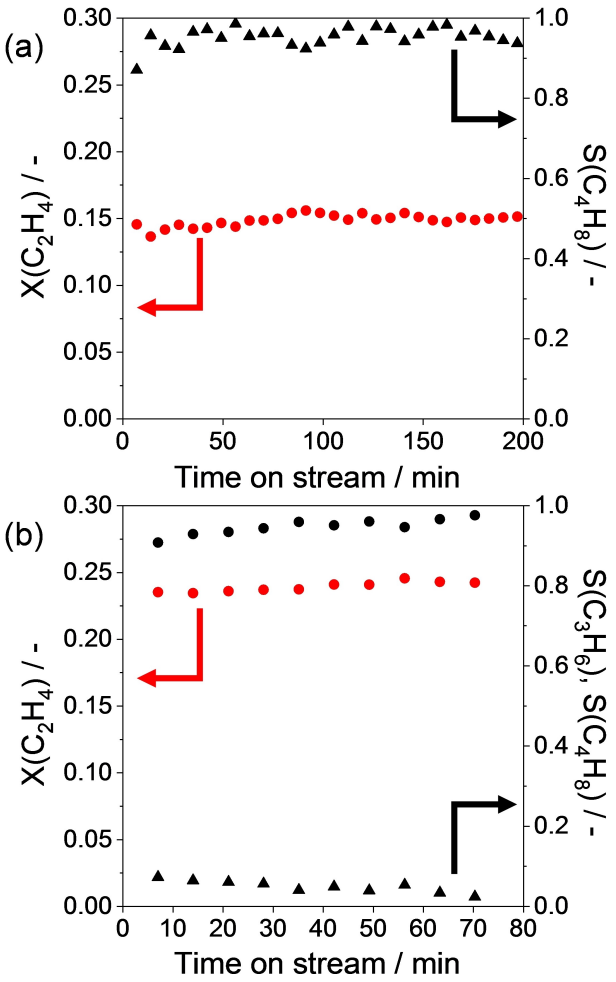

Figure 6. Temporal changes of ethylene conversion (red dots), selectivity to butenes (black triangles) and to propylene (black dots) determined at 150 °C over (a) Pd/Siral 40 (100 mg) and (b) Pd/Siral 40 (100 mg, upper layer) + Mo/Siral 40 (100 mg, bottom layer).

from 91 % to almost 98 %, while selectivity to butenes decreased from 7 % to 2 %. Such changes should be related to the in situ activation of metathesis catalyst.[17]

Conclusion

In summary, we have developed a highly efficient heterogeneous Pd-based catalyst for ethylene dimerization. Its activity is related to the presence of atomically dispersed Pd(II) species anchored through the vicinal hydroxyls of the Al_2O_3–SiO_2 support. The C–C coupling on Pd(II) species occurs through the Cossee-Arlman dimerization route, and the reaction barrier strongly depends on the local environment/geometry of the active sites. This knowledge provides an essential basis for the design and preparation of heterogeneous low-loaded metal catalysts for efficient ethylene dimerization. We also show the application potential of cascade conversion of ethylene to propylene when using the catalyst bed consisting of an ethylene-dimerization catalyst on top of an olefin-metathesis catalyst.

Supporting Information

The authors have cited additional references within the Supporting Information.[4a,6a,c,13,18]

Acknowledgements

The authors thank Dr. Stephan Bartling for performing XPS analysis, Anja Simmula for performing ICP analysis, Sebastian Smyczek for making selected catalyst fractions, and Dr. Dmitry E. Doronkin for the assistance in the analysis of XAS data. We acknowledge DESY (Hamburg, Germany) for the provision of experimental facilities and the state of Baden-Württemberg through bwHPC and the German Research Foundation (DFG) through grant no. INST 40/575-1 FUGG (JUSTUS 2 cluster, RVs bw17D011). The authors would like to extend their special thanks to Mikhail Kalinin and Elena Kalinina for the creation of the frontispiece picture for this article. Open Access funding enabled and organized by Projekt DEAL.

Conflict of Interest

The authors declare no conflict of interest.

Data Availability Statement

The data that support the findings of this study are available in the supplementary material of this article.

Keywords: Ethylene · Dimerization · Palladium · Heterogeneous Catalysis

[1] a) C. P. Nicholas, *Appl. Catal. A* **2017**, *543*, 82–97; b) A. M. Al-Jarallah, J. A. Anabtawi, M. A. B. Siddiqui, A. M. Aitani, A. W. Al-Sa′doun, *Catal. Today* **1992**, *14*, 1–121; c) A. V. Lavrenov, T. R. Karpova, E. A. Buluchevskii, E. N. Bogdanets, *Catal. Ind.* **2016**, *8*, 316–327.
[2] a) H. Li, S. Zhang, J. Zhou, Z. Wang, X. Zhao, T. Qiu, *Biofpr* **2022**, *16*, 1568–1582; b) Y. Liu, *Catalysts* **2018**, *8*, 537; c) J. V. Haveren, E. L. Scott, J. Sanders, *Biofpr* **2008**, *2*, 41–57.
[3] V. Hulea, *ACS Catal.* **2018**, *8*, 3263–3279.
[4] a) N. J. LiBretto, Y. Xu, A. Quigley, E. Edwards, R. Nargund, J. C. Vega-Vila, R. Caulkins, A. Saxena, R. Gounder, J. Greeley, G. Zhang, J. T. Miller, *Nat. Commun.* **2021**, *12*, 2322; b) Z. Xu, J. P. Chada, L. Xu, D. Zhao, D. C. Rosenfeld, J. L. Rogers, I. Hermans, M. Mavrikakis, G. W. Huber, *ACS Catal.* **2018**, *8*, 2488–2497.
[5] a) M. Ngcobo, S. O. Ojwach, *J. Mol. Catal.* **2021**, *508*, 111583; b) E. Rossetto, M. Caovilla, D. Thiele, R. F. de Souza, K. Bernardo-Gusmão, *Appl. Catal. A* **2013**, *454*, 152–159.
[6] a) C. Chen, M. R. Alalouni, X. Dong, Z. Cao, Q. Cheng, L. Zheng, L. Meng, C. Guan, L. Liu, E. Abou-Hamad, J. Wang, Z. Shi, K.-W. Huang, L. Cavallo, Y. Han, *J. Am. Chem. Soc.* **2021**, *143*, 7144–7153; b) E. D. Metzger, C. K. Brozek, R. J. Comito, M. Dincă, *ACS Cent. Sci.* **2016**, *2*, 148–153; c) E. D. Metzger, R. J. Comito, Z. Wu, G. Zhang, R. C. Dubey, W. Xu, J. T. Miller, M. Dincă, *ACS Sustainable Chem. Eng.* **2019**, *7*, 6654–6661; d) J. Ye, L. Gagliardi, C. J. Cramer, D. G. Truhlar, *J. Catal.* **2017**, *354*, 278–286; e) D. E. Ortega, *Chem. Eur. J.* **2021**, *27*, 10413–10421.
[7] H. Zhang, X. Li, Y. Zhang, S. Lin, G. Li, L. Chen, Y. Fang, H. Xin, X. Li, *Energy Environ. Focus* **2014**, *3*, 246–256.
[8] a) A. Finiels, F. Fajula, V. Hulea, *Catal. Sci. Technol.* **2014**, *4*, 2412–2426; b) J. R. Sohn, W. C. Park, D. C. Shin, *J. Mol. Catal. A* **2006**, *256*, 156–163; c) J. R. Sohn, W. C. Park, S.-E. Park, *Catal. Lett.* **2002**, *81*, 259–264; d) J. R. Sohn, W. C. Park, *Appl. Catal. A* **2002**, *230*, 11–18; e) J. R. Sohn, J. S. Lim, *Catal. Today* **2006**, *111*, 403–411; f) J. R. Sohn, S. H. Kwon, D. C. Shin, *Appl. Catal. A* **2007**, *317*, 216–225; g) J. R. Sohn, S. H. Lee, *Appl. Catal. A* **2007**, *321*, 27–34; h) Y. I. Pae, S. H. Lee, J. R. Sohn, *Catal. Lett.* **2005**, *99*, 241–248; i) M. Shin, H. Jeong, M.-J. Park, Y.-W. Suh, *Appl. Catal. A* **2020**, *591*, 117376.
[9] a) T. Yashima, Y. Ushida, M. Ebisawa, N. Hara, *J. Catal.* **1975**, *36*, 320–326; b) A. L. Lapidus, V. V. Mal′tsev, E. S. Shpiro, G. V. Antoshin, V. I. Garanin, K. M. Minachev, *B ACAD SCI USSR CH+* **1977**, *26*, 2275–2279; c) A. L. Lapidus, V. V. Mal'tsev, M. I. Maganya, V. I. Garanin, K. M. Minachev, *Acta Phys. Chem.* **1978**, *24*, 195–199; d) A. K. Ghosh, L. Kevan, *J. Am. Chem. Soc.* **1988**, *110*, 8044–8050; e) M. Hartmann, L. Kevan, *J. Phys. Chem.* **1996**, *100*, 4606–4611.
[10] Y. Li, D. Chen, X. Xu, X. Wang, R. Kang, M. Fu, Y. Guo, P. Chen, Y. Li, D. Ye, *Environ. Sci. Technol.* **2023**, *57*, 3467–3485.
[11] H. Bergna, W. Roberts, *Colloidal Silica: Fundamentals and Applications*, **2005**.
[12] R. Y. Brogaard, U. Olsbye, *ACS Catal.* **2016**, *6*, 1205–1214.
[13] a) A. N. Pestryakov, V. V. Lunin, S. Fuentes, N. Bogdanchikova, A. Barrera, *Chem. Phys. Lett.* **2003**, *367*, 102–108; b) L. S. F. Feio, C. E. Hori, S. Damyanova, F. B. Noronha, W. H. Cassinelli, C. M. P. Marques, J. M. C. Bueno, *Appl. Catal. A* **2007**, *316*, 107–116; c) J. Chen, Q. Zhang, Y. Wang, H. Wan, *ASC* **2008**, *350*, 453–464.
[14] J. Petit, L. Magna, N. Mézailles, *Coord. Chem. Rev.* **2022**, *450*, 214227.
[15] a) S. Debnath, S. Basu, B. M. Schmidt, J. J. Adams, N. Arulsamy, D. M. Roddick, *Polyhedron* **2020**, *181*, 114461; b) M. Navarro, V. Rosar, T. Montini, B. Milani, M. Albrecht, *Organometallics* **2018**, *37*, 3619–3630; c) S. D. Ittel, L. K. Johnson, M. Brookhart, *Chem. Rev.* **2000**, *100*, 1169–1204;

d) D. Roy, R. B. Sunoj, *Org. Biomol. Chem.* **2010**, *8*, 1040–1051.
[16] a) T. Hahn, U. Bentrup, M. Armbrüster, E. V. Kondratenko, D. Linke, *ChemCatChem* **2014**, *6*, 1664–1672; b) T. Otroshchenko, O. Reinsdorf, D. Linke, E. V. Kondratenko, *Catal. Sci. Technol.* **2019**, *9*, 5660–5667.
[17] K. Amakawa, S. Wrabetz, J. Kröhnert, G. Tzolova-Müller, R. Schlögl, A. Trunschke, *J. Am. Chem. Soc.* **2012**, *134*, 11462–11473.
[18] a) B. Ravel, M. Newville, *J. Synchrotron Radiat.* **2005**, *12*, 537–541; b) P. N. Plessow, *J. Chem. Theory Comput.* **2018**, *14*, 981–990; c) W. Daniell, U. Schubert, R. Glöckler, A. Meyer, K. Noweck, H. Knözinger, *Appl. Catal. A* **2000**, *196*, 247–260; d) K. Khivantsev, N. R. Jaegers, J.-H. Kwak, J. Szanyi, L. Kovarik, *Angew. Chem. Int. Ed.* **2021**, *60*, 17522–17530; e) T. Yang, R. Fukuda, S. Hosokawa, T. Tanaka, S. Sakaki, M. Ehara, *ChemCatChem* **2017**, *9*, 1222–1229; f) S. Moussa, P. Concepción, M. A. Arribas, A. Martínez, *Appl. Catal. A* **2020**, *608*, 117831; g) I. Ogino, B. C. Gates, *J. Am. Chem. Soc.* **2008**, *130*, 13338–13346; h) C. Invernizzi, T. Rovetta, M. Licchelli, M. Malagodi, *Int. J. Anal. Chem.* **2018**, *2018*, 7823248; i) C. Domingo, T. de los Arcos, A. Ainetschian, M. M. Sanz, I. Tanarro, *Vib. Spectrosc.* **2002**, *30*, 157–167.

Manuscript received: June 5, 2024
Accepted manuscript online: July 7, 2024
Version of record online: August 23, 2024